ChemComm

COMMUNICATION

Cite this: *Chem. Commun.*, 2022, **58**, 2886

Received 28th November 2021,
Accepted 25th January 2022

DOI: 10.1039/d1cc06681a

rsc.li/chemcomm

An indole-based fluorescent chemosensor targeting the autophagosome†

Sun Young Park,[a] Kyutae Kim,[b] Dong-Hyung Cho,[c] Eun-Young Jo,[b] Chulhun Kang*[b] and Min Hee Lee *[a]

Autophagy is a process for the degradation and recycling of intracellular components and dysfunctional organelles. We developed an indole-embedded fluorescent naphthalimide for the selective imaging of autophagosomes in live cells. It was shown as intense puncta in the fluorescence confocal images and co-localizes with an autophagosome marker, LC3-RFP. In addition, it was applied to cellular autophagic models based on ER stress and starvation to verify its capability.

Autophagy is a lysosome-dependent recycling process of unnecessary or dysfunctional cellular organelles such as mitochondria, endoplasmic reticulum, ribosomes, *etc.*[1] In autophagy,[2] autophagosomes are formed from a double-membrane, microtubule-associated protein 1A/1B-light chain 3 (LC3) and lipids, and in turn fuse with lysosomes for recycling *via* hydrolysis. Autophagy endows the cells with the restoration of damaged function or the reprogramming of cellular metabolism when cells adapt to altered cellular environments such as nutrient depletion, oxidative stress, *etc.*[3] Meanwhile, dysregulation of autophagy results in severe imbalances in cellular homeostasis and is associated with a vast range of human diseases, such as osteoarthritis, cancer, neurodegenerative diseases, infectious diseases, and even aging.[4] For these reasons, undoubtedly, autophagy monitoring is essential in a wide range of life sciences[5] and the techniques have been actively developed.[6–9]

Chemical probes have the advantage of being applied *in situ* to living cells under a variety of conditions with minimal disturbance of cell physiology relative to the biology-based technology. For example, adopting green fluorescent protein or other fluorescent proteins, which occasionally require transfection of the fused genes into the cells. The transfection procedure is relatively laborious and may push the cell physiology away from the intact one.[10] Recently, several fluorescent chemicals for monitoring autophagy in live cells have been developed.[11] They usually take advantage of chemical or physical alterations in the autophagosomes during the lysosomal fusion stage, such as pH, polarity or viscosity of the encapsulated components. However, it may be possible to point out that the targeted fluorescent changes may not be unique to autophagy alone, as they may be related to general features of activated lysosomes, *e.g.*, acidification and hydrolysis. Likely, a method based on direct sensing of autophagosomes would provide much enhanced reliability to the study of autophagy, which is rarely invented in the field of chemical probes.

In an effort to develop autophagosome-targeting probes, it was perceived that the indole moiety of tryptophan, an essential amino acid for humans, might be interesting as an autophagosome-targeting unit. The reasons are; (i) tryptophan and serotonin participate in autophagy regulation;[12] (ii) the indoles from gut metabolism have been suggested as endogenous regulators of autophagy;[13] and (iii) tryptophan residues are involved in protein–protein interactions involving LC3, a compelling autophagosome marker, during autophagosome formation.[14] In this context, we deduced indole-conjugated fluorescent molecules as an autophagosome-imageable chemical probe and its functional characterization in live cells was investigated. The probes comprise a naphthalimide and an indole moiety which are anticipated to act as a fluorescent reporter and a preferential binder to autophagosomes, possibly *via* interaction with LC3, respectively.[15] In addition, a linker between the two moieties adopts ethylene units to extend the emission wavelength. As illustrated in Scheme 1, the probe may visualize the autophagosomes in live cells *via* the interaction between the indole moiety and LC3.

The compound **1** was prepared from a naphthalimide derivative containing aldehyde **5** as depicted in Scheme 2 and Scheme S1 (ESI†). Briefly, after synthesizing **5** by adopting a literature procedure,[16] it was subjected to Wittig reaction with

[a] *Department of Chemistry, Sookmyung Women's University, Seoul 04310, Korea. E-mail: minheelee@sookmyung.ac.kr*
[b] *The School of East-West Medical Science, Kyung Hee University, Yongin 1104, Korea. E-mail: kangch@khu.ac.kr*
[c] *BK21 FOUR KNU Creative BioResearch Group, School of Life Sciences, Kyungpook National University, Daegu 41566, Korea*

† Electronic supplementary information (ESI) available. See DOI: 10.1039/d1cc06681a

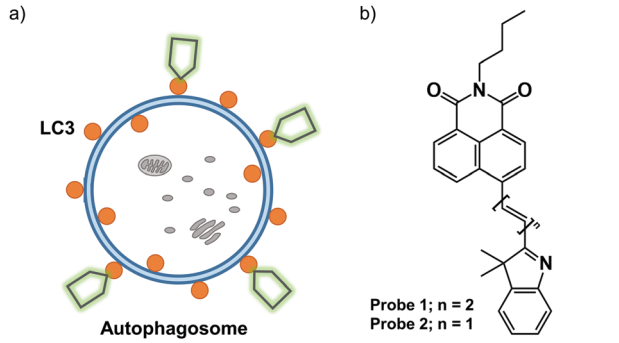

Scheme 1 (a) Schematic illustration of autophagosome imaging with the naphthalimide–indole system. (b) Chemical structure of the probe.

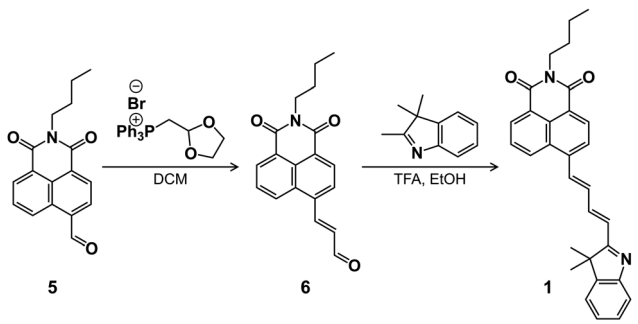

Scheme 2 Synthesis of naphthalimide–indole **1**.

(1,3-dioxolan-2-ylmethyl)triphenylphosphonium bromide in dichloromethane (DCM) to give intermediate **6**. And then, a condensation reaction of **6** and 2,3,3-trimethylindolenine in the presence of a catalytic amount of TFA in EtOH was performed to afford **1**. In addition, compound **2** was adopted as a reference to demonstrate the role of the indole moiety in this study and the synthetic route is described in Scheme S1 (ESI†). The chemical structures of **1** and **2** were identified by ^{1}H and ^{13}C NMR spectroscopy, as well as ESI-MS spectrometry (Fig. S1–S9, ESI†).

The absorption and emission spectra of the naphthalimide–indole compounds, **1** and **2**, were investigated in 1,4-dioxane. The absorption spectrum of **1** showed a maximum peak at 410 nm and that of **2** was observed at 350 nm (Fig. 1a). **1** showed an emission maximum ($\lambda_{max,em}$) at 560 nm upon excitation at 410 nm whereas **2** showed a maximum at 500 nm. The longer emission wavelength of **1** is attributed to the presence of an additional double bond compared to **2**. The solvatochromic fluorescence behavior of **1** shows a slight blue-shift with strong intensity in nonpolar solvents and a red-shifted spectrum with weak intensity in aqueous environments (Fig. 1b). In order to confirm the polarity-dependent blue shift with increasing fluorescence intensity of **1**, a 1,4-dioxane/water mixed system was used as a solvent, which indeed demonstrates a blue shift in a nonpolar environment (Fig. 1c). Quantum yields of **1** and **2** were measured in nonpolar and aqueous environments. The quantum yields of **1** and **2** in nonpolar solvent (1,4-dioxane) were 0.45 and 0.25. However, they were 0.0015 and 0.027 in aqueous solvent. Both **1** and **2** showed very strong fluorescence intensities in a nonpolar environment as opposed to aqueous environment. As a result, compound **2** showed a similar fluorescence feature under the corresponding conditions except that the emission wavelength is slightly shorter compared to **1**. In view of the spectroscopic properties of the compounds, subsequent biological studies have been concentrated on compound **1**.

Confocal microscopic investigation of probe **1** was performed in live HeLa cells. As expected, the cellular fluorescence intensity gradually increased and reached a plateau as the concentration of the probe increased from 0.1 to 1.0 μM (Fig. S10, ESI†). Interestingly, at higher concentrations, for example, 1.0 μM, the cell images show two different appearances, localized intense fluorescence spots (puncta) and hazy clouds widespread throughout the cytosolic space, which are indicated by white and yellow arrows in Fig. 2b, respectively. Further analysis using organelle trackers showed that the hazy clouds were associated with the endoplasmic reticulum (Fig. S11, ESI†). The puncta could be observed even with the 0.1 μM of probe, whereas cloud-like features were prominent at a high concentration of the probe (Fig. 2a). From these results, it is plausible that the puncta may be caused by a selective target of **1** and the clouds may be due to its random accumulation in the cells. Furthermore, the puncta were observed with probe **2** under similar conditions. Considering that the puncta

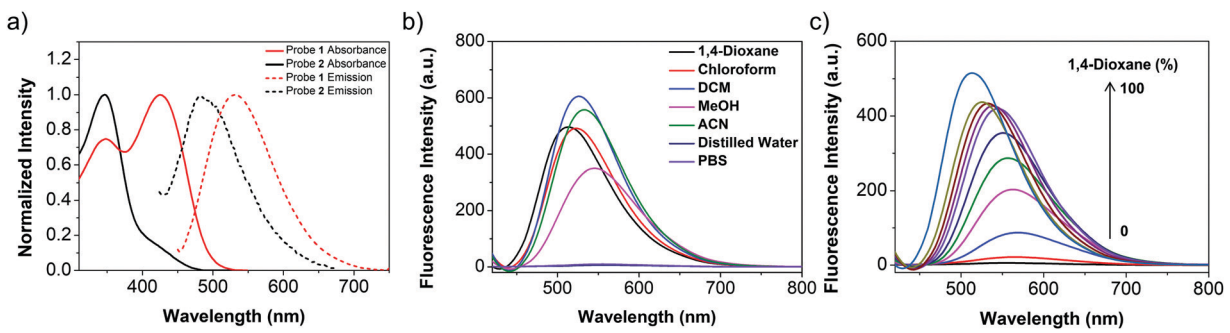

Fig. 1 (a) Absorption and emission spectra of **1** and **2** in 1,4-dioxane. (b) Emission spectra of **1** in various solvents. (c) Emission changes of **1** according to the 1,4-dioxane fraction in water. The excitation wavelengths were 410 nm and 350 nm for **1** and **2**, respectively. The concentrations of the compounds were 2.0 and 0.5 μM for the absorption and fluorescence spectra, respectively.

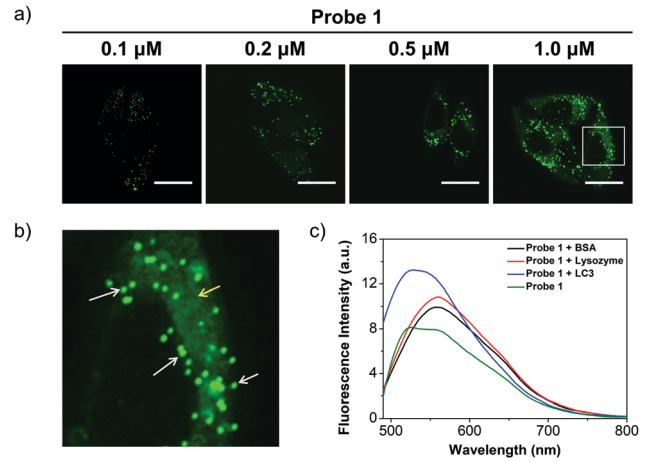

Fig. 2 (a) Confocal images of HeLa cells with different concentrations of **1** (0.1, 0.2, 0.5 and 1.0 μM) incubated for 20 min. (b) Enlarged image from the boxed area in (a) 1.0 μM. Confocal images were recorded using a 458 nm excitation laser and an emission band-pass filter of 475–525 nm (pseudo green color). Scale bar = 20 μm. (c) Fluorescence spectra of probe **1** in the presence of LC3, BSA, and lysozyme for 30 min in PBS solution.

are typical of an autophagosome's appearance, the results in Fig. 2 strongly suggest that probe **1** may detect autophagosomes in living cells.

To explore further whether probe **1** is indeed capable of monitoring the autophagosome, a spectroscopic measurement of probe **1** with LC3, a prominent autophagosome marker, was performed and compared to those with bovine serum albumin (BSA) and lysozyme, in PBS solution, and the result is shown in Fig. 2c. In the presence of BSA or lysozyme, the fluorescence intensity of the probe slightly increased where $\lambda_{max,em}$ was around 560 nm. However, with LC3, the emission was blue-shifted to 530 nm with a further increase in fluorescence intensity. These results indicate that there is a distinctive interaction between LC3 and the probe, which differs from those with BSA or lysozyme. Considering that LC3 locates on the surface of early autophagosomes[17] and has an affinity to indole-containing compounds,[15] this result supports probe **1**'s putative capability as an autophagosome sensor.

To confirm the autophagosome selectivity of probe **1** in living cells, colocalization of the probe was performed using confocal microscopy with various organelle-selective fluorescent markers. They include mitochondria, lysosome, endoplasmic reticulum, early endosome and late endosome markers, and LC3-RFP was used as an autophagosome marker. The results are shown in Fig. S12 and S13 (ESI†). They show that none of the makers' images significantly overlap with probe **1**'s image, where the Pearson's Correlation Coefficient was in fact less than 0.2 (Fig. S12, ESI†). And, its overlay with the autophagosome marker was terribly poor (ESI,† Fig. S13, panel a); however, the colocalizing image for LC3-RFP has an interesting feature. The intensity of probe **1** is very weak in the region with high intensity of LC3-RFP emission; in contrast, the probe's emission is strong in the region with weak LC3-RFP emission. A similar feature was further confirmed in the fluorescence microscopic image (ESI,† Fig. S13 panel b). These results strongly raise a possibility of proximal location of probe **1** to LC3-RFP in cells so that the RFP quenched the probe's emission, which can be easily demonstrated by fluorescence resonance energy transfer (FRET) between them.

In order to pursue the colocalization of autophagosomes and probe **1**, FRET between probe **1** and LC3-RFP was investigated. Basically, the emission spectrum of probe **1** and the absorption spectrum of RFP overlapped significantly (Fig. 3a). In Fig. 3b, the FRET image obtained from excitation at 458 nm with a 650 nm emission long-path filter indeed showed bright puncta, but these were not visible in the corresponding images of probe **1** or LC3-RFP alone (Fig. 3c). In the figure, not all cells exhibit FRET, which may be due to the presence of an untransfected population of cells, which is one of the general characters of gene transfection.[18] Nonetheless, these results indicate that probe **1** is located very close to the LC3 of the cells, considering that FRET can occur if the two fluorophores

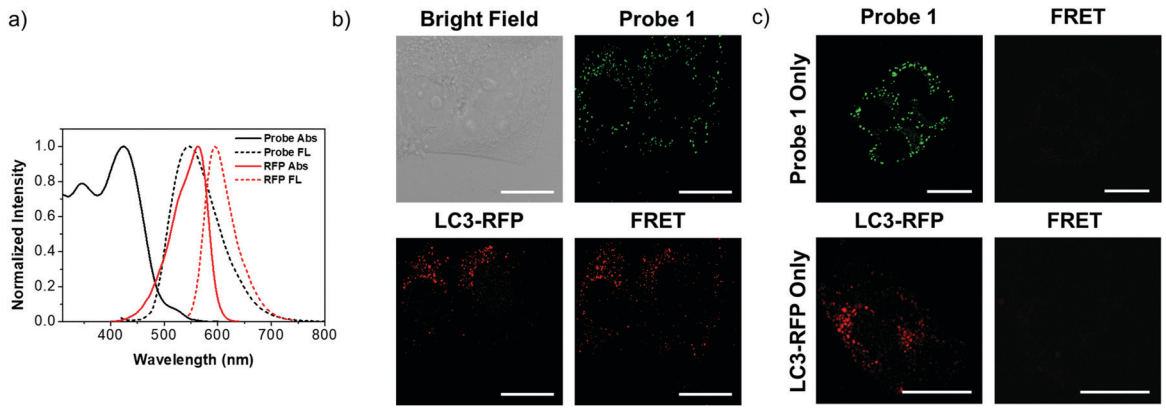

Fig. 3 (a) Spectral overlap between the emission of probe **1** and the absorption of RFP. (b) FRET between probe **1** and LC3-RFP in cells. The HeLa cells were transfected with LC3-RFP and incubated with probe **1** (0.1 μM). (c) Probe **1**-treated HeLa cells and LC3-RFP transfected HeLa cells. The excitation/emission filter combinations for probe **1**, LC3-RFP and FRET were 458 nm/475–525 nm band-pass, 543 nm/650 nm long-pass and 458 nm/650 nm long-pass, respectively.

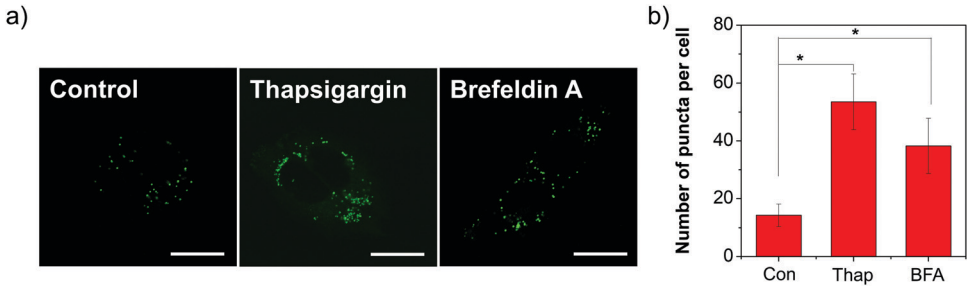

Fig. 4 Confocal images of probe **1** in ER-stressed HeLa cells by thapsigargin and brefeldin A. (a) HeLa cells were treated with thapsigargin (5 μM) and brefeldin A (100 μM) for 2 h and then with probe **1** (0.1 μM, 20 min). Confocal images were recorded by using a 543 nm laser and a 475–525 nm emission band-pass filter. (b) Numbers of puncta per cell in the images are presented in the histogram. * indicates $P < 0.05$, and $n = 4$.

are located below 3–5 nm. Altogether, it is highly plausible that probe **1** selectively visualizes autophagosomes, presumably through preferential interaction with LC3.

Verification of probe **1** as a potent autophagosome sensor would require its application to cellular autophagic models. This was attempted using confocal microscopy and chemically induced ER-stress models involving autophagy where the results are shown in Fig. 4. Thapsigargin and brefeldin A are known to induce ER stress *via* inhibitory effects on ER Ca^{2+} ATPase, and on the transport of the newly synthesized proteins from the ER to the Golgi complex, respectively.[19,20] Under these ER stress conditions, as shown in Fig. 4, the number of puncta dramatically increased, and is 3.8 and 2.7-fold compared to that of the untreated control group. This result verifies the capability of probe **1** as an excellent chemical marker for autophagosomes. Additionally, to confirm that probe **1** can detect autophagosomes in cells, autolysosome fusion inhibitor bafilomycin A1 was used (Fig S14, ESI†).[21] To induce autophagy, glucose in the media was deprived by using Hank's balanced salt solution (HBSS),[22] resulting in a slight increase of the fluorescent puncta. Upon further treatment of bafilomycin A1, the fluorescence intensity in the cells was dramatically increased. These results further demonstrated that probe **1** can readily visualize autophagosomes as fluorescent puncta.

In conclusion, the fluorescent emission of probe **1** increases in an aqueous environment and it is blue-shifted by 30 nm in the presence of LC3, an autophagosome marker. And, in the live HeLa cells, probe **1** appears as intense and distinct fluorescence spots in confocal microscopic images and co-localizes with LC3, which was evident from FRET between probe **1** and LC3-fused RFP. Finally, its application to an ER stress model using thapsigargin and brefeldin A, as well as a starvation model using bafilomycin A1, demonstrates the increase in the number of autophagosomes in cells, which verifies that probe **1** is a selective chemical sensor for autophagosomes.

This research was supported by the National Research Foundation of Korea (NRF) grant funded by the Korean government (MSIT) (2021R1F1A1045790, M. H. L.).

Conflicts of interest

There are no conflicts to declare.

Notes and references

1 C. de Duve, *Eur. J. Biochem.*, 1983, **137**, 391–397.
2 K. R. Parzych and D. J. Klionsky, *Antioxid. Redox Signaling*, 2014, **20**, 460–473.
3 G. Filomeni, D. De Zio and F. Cecconi, *Cell Death Differ.*, 2015, **22**, 377–388.
4 B. Levine and G. Kroemer, *Cell*, 2008, **132**, 27–42.
5 D. J. Klionsky, A. Kamal Abdel-Aziz, S. Abdelfatah, M. Abdellatif, A. Abdoli and S. Abel, *et al.*, *Autophagy*, 2021, **17**, 1–382.
6 H. Kim, H. Kim, J. Choi, K.-S. Inn and J. Seong, *ACS Sens.*, 2020, **5**, 3850–3861.
7 X. Li, X. Liang, J. Yin and W. Lin, *Chem. Soc. Rev.*, 2021, **50**, 102–119.
8 P. Ning, Y. Feng, Y. Ding, L. Bai, L. Li, H. Yu, X. Meng and L. Hou, *Anal. Chem.*, 2018, **90**, 7122–7126.
9 M. H. Lee, N. Park, C. Yi, J. H. Han, J. H. Hong, K. P. Kim, D. H. Kang, J. L. Sessler, C. Kang and J. S. Kim, *J. Am. Chem. Soc.*, 2014, **136**, 14136–14142.
10 L. Jacobsen, S. Calvin and E. Lobenhofer, *Biotechniques*, 2009, **47**, 617–624.
11 (*a*) Y. Liu, L. Teng, L. Chen, H. Ma, H. W. Liu and X. B. Zhang, *Chem. Sci.*, 2018, **9**, 5347–5353; (*b*) X. Li, Y. Hu, X. Li and H. Ma, *Anal. Chem.*, 2019, **91**, 11409–11416; (*c*) X. Li, X. Li and H. Ma, *Chem. Sci.*, 2020, **11**, 1617–1622.
12 (*a*) C. Hunt, X. Zhao, Z. Crisp, K. Choi, P. de Figueiredo, A. Jayaraman, J. Karpac and R. C. Alaniz, *J. Immunol.*, 2017, **198**, 6217; (*b*) C. Soll, J. H. Jang, M. O. Riener, W. Moritz, P. J. Wild, R. Graf and P. A. Clavien, *Hepatology*, 2010, **51**, 1244–1254.
13 M. A. Pappolla, G. Perry, X. Fang, M. Zagorski, K. Sambamurti and B. Poeggeler, *Neurobiol. Dis.*, 2021, **156**, 105403.
14 (*a*) A. Rozenknop, V. V. Rogov, N. Y. Rogova, F. Löhr, P. Güntert, I. Dikic and V. Dötsch, *J. Mol. Biol.*, 2011, **410**, 477–487; (*b*) T. Kouno, M. Mizuguchi, I. Tanida, M. Hirata, E. Kominami and K. Kawano, *J. Biol. Chem.*, 2005, **280**, 24610–24617.
15 Y. Thielmann, J. Mohrlüder, B. W. Koenig, T. Stangler, R. Hartmann, K. Becker, H.-D. Hçltje and D. Willbold, *Chem. Bio. Chem.*, 2008, **9**, 1767–1775.
16 J. Lee and M. H. Lee, *Tetrahedron Lett.*, 2017, **58**, 3178–3182.
17 G. Runwal, E. Stamatakou, F. H. Siddiqi, C. Puri, Y. Zhu and D. C. Rubinsztein, *Sci. Rep.*, 2019, **9**, 10147.
18 T. A. Kost and C. W. Kemp, *Adv. Exp. Med. Biol.*, 2016, **896**, 187–197.
19 M. Høyer-Hansen and M. Jäättelä, *Cell Death Differ.*, 2007, **14**, 1576–1582.
20 P. Purhonen, K. Pursiainen and H. Reunanen, *Eur. J. Cell Biol.*, 1997, **74**, 63–67.
21 C. Mauvezin and T. P. Neufeld, *Autophagy*, 2015, **11**, 1437–1438.
22 B. Levine and G. Kroemer, *Cell*, 2008, **132**, 27–42.